Electronic distribution in superlattice quantum cascade lasers

Mariano Troccoli, Gaetano Scamarcio,[a] and Vincenzo Spagnolo
INFM, Dipartimento Interateneo di Fisica, Università e Politecnico di Bari, via Amendola 173, 70126 Bari, Italy

Alessandro Tredicucci, Claire Gmachl, Federico Capasso, Deborah L. Sivco, and Alfred Y. Cho
Bell Laboratories, Lucent Technologies, 600 Mountain Avenue, Murray Hill, New Jersey 07974

Marinella Striccoli
Centro Laser s.r.l., Strada Provinciale per Casamassima, Valenzano, Bari, Italy

(Received 17 April 2000; accepted for publication 27 June 2000)

The electron population in the excited miniband of quantum cascade structures with intrinsic superlattice active regions is extracted from the fine structure analysis of spontaneous interminiband electroluminescence spectra. At current densities typical of laser thresholds, the electrons injected into the excited miniband of a $(GaInAs)_{6\,nm}/(AlInAs)_{1.8\,nm}$ superlattice are described by a nonequilibrium thermal distribution characterized by temperatures $T_e > 200\,K$, much higher than the lattice temperature $T_L = 15\,K$. © *2000 American Institute of Physics.* [S0003-6951(00)04534-4]

The quantum cascade laser (QCL) is a new midinfrared semiconductor source based on electronic transitions between energy levels created in the conduction band by quantum confinement.[1] Emission of radiation is obtained by tunnel injection of electrons into high energy excited subbands or minibands.[2–5] In QCLs with periodic superlattice (SL) active regions, a model assuming that injected electrons form a thermalized distribution at the bottom of the second miniband[3,4] gives estimates of laser threshold currents in agreement with the experimental values and is being successfully used for the rapid development of these devices. However, for a complete description of population inversion and optical gain, the actual electron energy distribution is needed. Below laser threshold, excited electrons relax their excess energy via electron–optical phonon and electron–electron scattering processes. At large injected currents, when the power given to the excited electron system exceeds the energy relaxation rate, a nonequilibrium (hot) electron ensemble with average energy higher than the thermal reservoir can be created.[6]

In this letter, we show that the energy distribution of electrons in quantum cascade structures with periodic superlattice active regions can be directly determined from the analysis of interminiband electroluminescence. We compared the two significant regimes of low and high powers corresponding to low current densities ($J < 100\,A/cm^2$) and current densities close to typical QCL thresholds ($J > 1\,kA/cm^2$). In the latter case, we found that a hot carrier distribution is sustained in the excited miniband, and that this distribution can be described by a temperature T_e.

Figure 1 shows the energy dispersion of a $(GaInAs)_{L_w}/(AlInAs)_{L_b}$ infinite SL with $L_w = 6.0\,nm$ and $L_b = 1.8\,nm$, calculated in the framework of a Kronig–Penney model. The energy levels of a nine periods SL, calculated from the numerical solution of the Schrödinger equation, sample the infinite SL dispersion. These levels are labeled with the indices $i, j = 1-9$ in Fig. 1 starting from states at the minigap. Selection rules calculated assuming flat bands (zero electric field) show that only vertical interminiband transitions with $i = j$ are allowed. In this case, there is a clear correspondence between emitted photon energies and interminiband transition. This fact can be exploited to unambiguously extract the individual subband populations in the second miniband from the interminiband luminescence spectrum at energies higher than the minigap. In contrast, extensive electric field penetration in the SL gives non-negligible oscillator strength to diagonal ($i \neq j$) transitions and makes uncertain the assignments of spectral features. The analysis of the high energy portion of the interminiband luminescence spectrum relies on the opposite k_z dispersion in the first two minibands of a periodic SL. Similarly, the electronic temperature is readily extracted from the high energy tail of interband (conduction-to-valence) luminescence.[7]

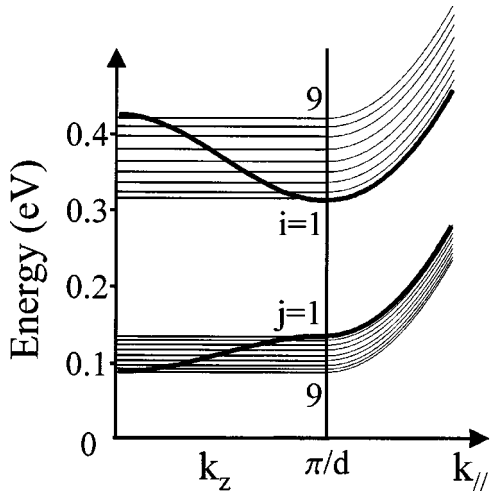

FIG. 1. Calculated energy dispersion as a function of wave vector along the growth axis (k_z) and in-plane wavevector ($k_{||}$) for a GaInAs/AlInAs superlattice with $L_w = 6.0\,nm$, $L_b = 1.8\,nm$. Bold line: infinite superlattice. Thin lines: finite superlattice with nine periods. In the latter case, energy levels are labeled with indexes $i, j = 1-9$ starting from states at the minigap.

[a]Electronic mail: scamarcio@fisica.uniba.it

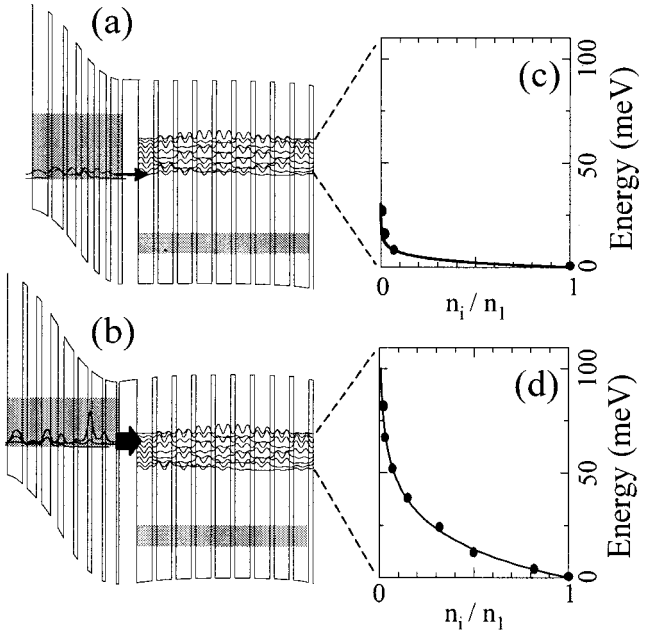

FIG. 2. Band structure of one period (injector and SL regions) of samples D2552 (a) and D2551 (b) calculated at heat sink temperature $T=15$ K with total applied voltages $U=1.38$ and 1.88 V, respectively. The active region is a nine period GaInAs/AlInAs undoped superlattice with $L_w=6.0$ nm and $L_b=1.8$ nm. The layer sequence in the injectors is (dimensions in nm) 1.5/**4.3**/1.6/**3.3**/2.1/**2.4**/2.4/**2**/2.6/**1.8**/2.8/**1.6**/6.8 for D2552 and 1.8/**3.6**/2/**3.4**/3/**2.4**/3.8/**1.6**/3.9/**1.5**/4.2/**1.2**/4.3/**1.1**/6.8 for D2551. Bold: InGaAs wells. Underlined: *n* doping with $[\mathrm{Si}]=5\times10^{17}$ cm^{-3}. Shadowed areas represent the first miniband in the injector and SL regions, while the wave functions square moduli of the excited SL miniband are traced. (c) and (d): electronic energy distributions in the excited miniband, determined from the analysis of the electroluminescence spectra of Fig. 4. Dots: relative subband occupation. Continuous line: interpolation by a Boltzmann distribution with $T_e=35$ K (c) and $T_e=204$ K (d).

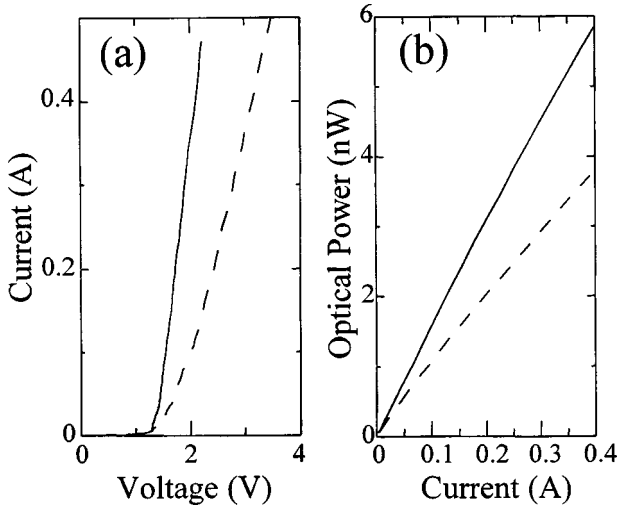

FIG. 3. Measured current–voltage (a) and optical power as a function of drive current (b) characteristics of sample D2551 (solid line) and D2552 (dashed line) at $T=15$ K.

In order to compare different injected currents while preserving flat-bands in the SL we designed two $Ga_{1-x}In_xAs/Al_{1-y}In_yAs$[8] quantum cascade structures with different injectors and identical SL active regions. The undoped SL is composed of nine periods with $L_w=6.0$ nm and $L_b=1.8$ nm. The layer sequences in the injectors are designed to keep flat bands in the SL either with standard tunnel injection close to the bottom of the second miniband [sample D2552, see Fig. 2(a)] or with injection into high energy states close to the top of the second miniband [sample D2551, see Fig. 2(b)]. Each sample consists of five SLs interleaved with six injectors and was grown on semi-insulating InP substrate by molecular beam epitaxy. The band structures of Fig. 2 were calculated by iteratively solving Poisson and Schroedinger equations until self-consistence between electron potential and charge distribution is achieved. In both cases great care has been taken to appropriately choose selective doping of the injectors (see caption of Fig. 2) to completely screen the electric field in the SL and avoid miniband breaking due to field penetration,[9] following the guidelines of Refs. 4 and 10.

The current–voltage characteristics of Fig. 3,[11] show that the turn-on voltage is 1.23 V for both structures. The corresponding applied voltage per period is very close to the expected value $(E_{i=1}-E_{F,n})/q$, where $E_{i=1}$ is the energy of the lowest excited subband, $E_{F,n}$ is the quasi-Fermi level and q is the electron charge. As a result of the increased injection rate, sample D2551 exhibits a much sharper turn-on and a differential resistance value of 1.9 Ω, a factor of two smaller than D2552 (3.6 Ω). From the L–I curves of Fig. 3(b), showing the measured midinfrared optical power as a function of the current, we measure a slope efficiency of 15 nW/mA for sample D2551, larger than the corresponding value for D2552 (9 nW/mA).

Figure 4(a) shows the electroluminescence spectrum of sample D2552, collected at a heat sink temperature $T=15$ K, at an applied voltage of 1.38 V($J=73$ A/cm^2), corresponding to the band diagram of Fig. 2(a). The emission spectrum is characterized, as expected,[12] by a single peak at 179 meV with a FWHM of 24 meV, associated with inter-miniband transitions at the minigap $(i=j=1)$. The electroluminescence spectrum of sample D2551 in Fig. 4(b) is

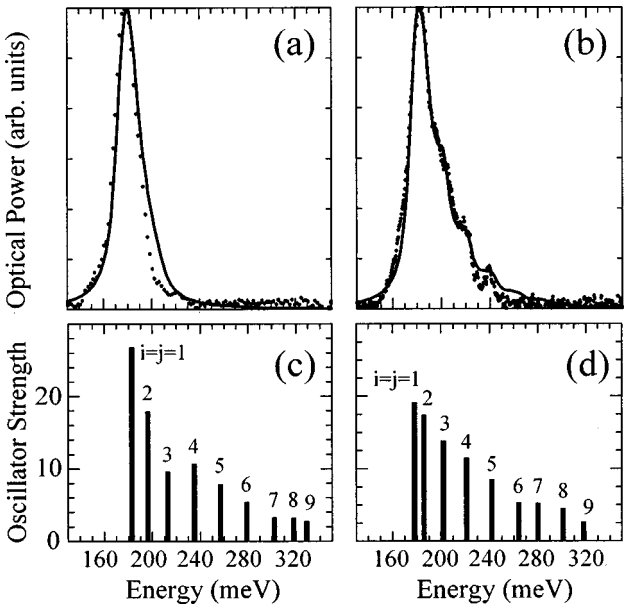

FIG. 4. Electroluminescence spectra of samples D2552 (a) and D2551 (b) collected at 1.38 V, 13 mA (a) and 1.88 V, 0.3 A (b). The heat sink temperature is $T=15$ K. Dots: experimental data; solid line: calculated spectra. Calculated oscillator strengths for $i-j$ transitions for sample D2552 (c) and D2551 (d).

recorded at 1.88 V, corresponding to a flat-band condition in the SL, as shown in Fig. 2(b). The resultant current density $J=1.7\,\mathrm{kA/cm^2}$ is comparable with typical QCL thresholds.[4,5] The main peak at 183 meV is the convolution of transitions 1–1 and 2–2, with energies 178 and 186 meV, closest to the minigap. Additional peaks at 200, 220, and 240 meV arise from interminiband transitions with $i=j=3$, 4, and 5, respectively, and reveal substantial population of high energy levels of the second miniband under steady state injection.

Based on the calculated quasi-Fermi level, 4 meV above the SL ground state, one can assume negligible population of first miniband levels with $j<8$. Accordingly, the luminescence lineshape can be written as

$$P_L(\hbar\omega)=\eta_C N_P \sum_{i=1}^{9}\sum_{j=1}^{9} n_i \frac{\hbar\omega_{ij}}{\tau_{ij}^{SP}}\mathcal{L}(\hbar\omega), \tag{1}$$

where n_i are the subband populations in the second miniband, η_C is the collection efficiency ($\sim 2\times10^{-3}$), N_P is the number of periods of the cascade structure, and $\mathcal{L}(\hbar\omega)$ is the Lorentzian lineshape with a phenomenological broadening $\Gamma/2=12\,\mathrm{meV}$, as measured in sample D2552. The spontaneous lifetimes τ_{ij}^{SP} are related with the oscillator strengths f_{ij} by the expression:

$$(\tau_{ij}^{SP})^{-1}=\frac{e^2\omega_{ij}^3 n}{\pi\hbar\varepsilon_0 c^3}|\langle\psi_i|z|\psi_j\rangle|^2=\frac{e^2\omega_{ij}^2 n}{2\pi m_0\varepsilon_0 c^3}f_{ij}, \tag{2}$$

where n is the effective refractive index, $\hbar\omega_{ij}$ is the transition energy, m_0 is the free electron mass, and Ψ_{ij} are the electron wave functions. The calculated f_{ij} are shown in Figs. 4(c) and 4(d). Owing to the flat band condition associated with the appropriate injector design, the oscillator strengths of vertical transitions ($i=j$) are dominant.

Fitting the luminescence lineshape (1) to the experimental spectra yields the relative excited subband populations n_i/n_1 shown in Figs. 2(c) and 2(d). Under high current injection [sample D2551, Fig. 4(b)] the subband populations can be interpolated by a Maxwell–Boltzmann distribution $n_i/n_1\sim\exp(-E_i/kT_e)$ with a single electronic temperature $T_e=204\,\mathrm{K}$. At larger current densities of 5.3 and 7.2 $\mathrm{kA/cm^2}$, close to reported thresholds in QCLs with periodic SLs,[3,10] the applied voltages (2.75 and 3.3 V) cause a partial field penetration in the active region. The analysis of the high-energy structure of the electroluminescence spectra gives electronic temperatures $T_e=260$ and 350 K, respectively. At low injected currents in D2552, we estimate an electronic temperature $T_e<35\,\mathrm{K}$ [Fig. 2(c)] since we observe luminescence only from the lowest excited subband. At the same current density of Fig. 4(b) (1.7 $\mathrm{kA/cm^2}$) sample D2552 shows a broad luminescence spectrum extending up to 360 meV with a structure associated with vertical and diagonal interminiband transitions, due to strong field penetration. The main spectral features can be reproduced with $T_e>200\,\mathrm{K}$. It is important to stress that negligibly small lattice heating occurs in our samples at the injected power levels of Figs. 2 and 4 (<0.3 W). In fact, we measured a lattice temperature increase $\Delta T_L<15\,\mathrm{K}$ by microprobe photoluminescence spectroscopy in QCL devices at operating powers of 1 W.[13]

The above results suggest that in our structures, at high injected current levels, electron–electron scattering processes are fast enough to establish a Maxwell–Boltzmann distribution in the excited miniband. In fact, at electron densities $\sim10^{10}-10^{11}\,\mathrm{cm^{-2}}$, electron–electron scattering rates[14] comparable or higher than the electron–optical phonon ones are expected. At 1.7 $\mathrm{kA/cm^2}$, the energy loss rate per electron due to longitudinal optical phonon emission at the measured electronic temperature $T_e=204\,\mathrm{K}$, estimated as: $\langle dE/dt\rangle=\hbar\omega_{LO}/\tau_{LO}\exp(-\hbar\omega_{LO}/kT_e)\approx5\,\mathrm{nW}$, is equal to the injected power per electron obtained sharing the electrical power among the SL electrons only, and using $n_{SL}=10^{11}\,\mathrm{cm^{-2}}$ given by our self-consistent calculation. This agreement can be explained considering that the electrons gain and relax their excess energy mainly in the SL region and suggests a local variation of the electronic temperature.

This work was partly supported by INFM project PRA-SUPERLAS and MURST-CIPE Cl.26P5BW2. The authors gratefully acknowledge C. Giannini and L. Tapfer for x-ray analysis, A. Valentini and G. Casamassima for contacts evaporation and annealing, P. Tempesta for device bonding, and P. Lugli for valuable discussions.

[1] F. Capasso, C. Gmachl, A. Tredicucci, D. L. Sivco, A. L. Hutchinson, and A. Y. Cho, Opt. Photonics News **10**, 31 (1999).
[2] J. Faist, F. Capasso, D. L. Sivco, C. Sirtori, A. L. Hutchinson, and A. Y. Cho, Science **264**, 553 (1994).
[3] G. Scamarcio, F. Capasso, C. Sirtori, J. Faist, A. L. Hutchinson, D. L. Sivco, and A. Y. Cho, Science **276**, 773 (1997).
[4] F. Capasso, A. Tredicucci, C. Gmachl, D. L. Sivco, A. L. Hutchinson, A. Y. Cho, and G. Scamarcio, IEEE J. Sel. Top. Quantum Electron. **5**, 792 (1999).
[5] C. Gmachl, F. Capasso, A. Tredicucci, D. L. Sivco, R. Köhler, A. L. Hutchinson, and A. Y. Cho, IEEE J. Sel. Top. Quantum Electron. **5**, 808 (1999).
[6] For a comprehensive review on hot electron phenomena see *Hot Electrons in Semiconductors: Physics and Devices*, edited by N. Balkan (Clarendon, Oxford, 1998).
[7] J. Shah, A. Pinczuk, A. C. Gossard, and W. Wiegmann, Phys. Rev. Lett. **54**, 2045 (1985).
[8] For the In mole fractions, we used the values $x=0.55$ and $y=0.49$, assessed by x-ray diffraction and Raman scattering characterizations. These values, slightly different from lattice matched ones, correspond to a practically negligible 0.3% strain.
[9] G. Scamarcio, M. Troccoli, F. Capasso, A. L. Hutchinson, D. L. Sivco, and A. Y. Cho, *Proceedings of the 24th International Conference on the Physics of Semiconductors (ICPS 24)* (World Scientific, Singapore, 1998).
[10] A. Tredicucci, F. Capasso, C. Gmachl, D. L. Sivco, A. L. Hutchinson, A. Y. Cho, J. Faist, and G. Scamarcio, Appl. Phys. Lett. **72**, 2388 (1998).
[11] The samples were processed into 150-μm-diam mesas with alloyed ohmic contacts. The substrate was wedged at 45° to facilitate light collection. The devices, indium soldered onto copper holders and mounted into a closed-cycle He cryostat with ZnSe windows, were voltage driven at 40 kHz with 50% duty cycle. Midinfrared electroluminescence spectra were collected with an FTIR spectrometer operating in the step scan and lock-in mode, using ZnSe $f/1$ optics and a cooled HgCdTe detector.
[12] G. Scamarcio, F. Capasso, J. Faist, C. Sirtori, D. L. Sivco, A. L. Hutchinson, and A. Y. Cho, Appl. Phys. Lett. **70**, 1796 (1997).
[13] V. Spagnolo, M. Troccoli, and G. Scamarcio (unpublished results).
[14] S.-C. Lee, I. Galbraith, and C. R. Pidgeon, Phys. Rev. B **52**, 1874 (1995).